Turbulent transport in hydromagnetic flows

Turbulent transport in hydromagnetic flows

A Brandenburg[1,2]**, P Chatterjee**[1]**, F Del Sordo**[1,2]**, A Hubbard**[1]**,
P J Käpylä**[1,3] **and M Rheinhardt**[1]

[1] NORDITA, Roslagstullsbacken 23, SE-10691 Stockholm, Sweden
[2] Department of Astronomy, Stockholm University, SE-10691 Stockholm, Sweden
[3] Department of Physics, FI-00014 University of Helsinki, Finland

E-mail: brandenb@nordita.org

Abstract
The predictive power of mean-field theory is emphasized by comparing theory with simulations under controlled conditions. The recently developed test-field method is used to extract turbulent transport coefficients both in the kinematic and the nonlinear or quasi-kinematic cases. A striking example of the quasi-kinematic method is provided by magnetic buoyancy-driven flows that produce an α effect and turbulent diffusion.

(Some figures in this article are in colour only in the electronic version.)

1. Introduction

What happens when fluids mix? What if a fluid is moving in a magnetized environment? Are there analogies between the motion of a cloud in the sky, milk in a coffee cup and solar flares? The study of fluids and magnetic fields has always been a challenging branch of physics, leading to the development of tools of wide applicability, from meteorology to the study of galaxies. In particular, the connection between the existence of fluids in motion and the amplification of magnetic fields has been investigated both analytically and experimentally since the beginning of the 20th century. This generation of a magnetic field by dynamo action was already proposed by Larmor (1919), but a proper understanding of such a process requires both physical insight and a theoretical framework that describes the magneto-hydrodynamical (MHD) context in which the phenomena occur. The most common theoretical approach to MHD dynamos is the application of mean-field theory (Parker 1955, Steenbeck and Krause 1969, Moffatt 1978, Parker 1979, Krause and Rädler 1980). The core concept on which mean-field theory (hereafter MFT) rests is that turbulent systems (which include most natural MHD dynamos) are often amenable to a two-scale approach, where the velocity and magnetic fields are decomposed into mean and fluctuating components: $U = \overline{U} + u$ and $B = \overline{B} + b$. The mean parts $\overline{U}$ and $\overline{B}$ generally vary slowly both in space and time, and capture the global behavior of the system, which is often also the observable one. The fluctuating fields, on the other hand, describe irregular, often chaotic small-scale effects.

Using the aforementioned decomposition the equation for the time evolution of the magnetic field, known as the induction equation, can be rewritten as a set of two equations for mean and fluctuating quantities

$$\frac{\partial \overline{B}}{\partial t} = \nabla \times \left(\overline{U} \times \overline{B} \right) + \nabla \times \overline{\mathcal{E}} + \eta \nabla^2 \overline{B}, \tag{1}$$

$$\frac{\partial b}{\partial t} = \nabla \times \left(\overline{U} \times b \right) + \nabla \times \left(u \times \overline{B} \right) + \nabla \times (u \times b)' + \eta \nabla^2 b, \tag{2}$$

where η is the microphysical magnetic diffusivity of the fluid (here assumed uniform), while $\overline{\mathcal{E}} \equiv \overline{u \times b}$ is the mean electromotive force, and $(u \times b)' = u \times b - \overline{u \times b}$.

Correlations such as $\overline{u \times b}$ are at the heart of turbulent transport, and apply to a broad range of processes, from dynamos to the mixing of chemicals through stirring. For example, the evolution of the mean $\overline{C}$ of a chemical concentration $C = \overline{C} + c$ is governed by the mean flux $\overline{uc}$ resulting from the interplay of the fluctuations. Likewise, the evolution of mean momentum, $\rho \overline{U}$, is governed by the Reynolds stress, $\rho \overline{u_i u_j}$ (with constant density ρ). We return to the flux of chemicals at the end of section 4.1. Here, the key task consists in relating the mean emf $\overline{\mathcal{E}}$ to the mean

field $\overline{\boldsymbol{B}}$. Underlying symmetries that constrain the form of this relation are of significant help. $\overline{\boldsymbol{\mathcal{E}}}$ is a vector, so if the system is homogeneous and the turbulence isotropic, in what direction can it point? The answer is that in such a system $\overline{\boldsymbol{\mathcal{E}}}$ can have constituents pointing along the mean magnetic field $\overline{\boldsymbol{B}}$ and the mean current density $\overline{\boldsymbol{J}} = \nabla \times \overline{\boldsymbol{B}}/\mu_0$ (as well as higher-order spatial and time derivatives, see section 4.2), which leads to approximations such as

$$\overline{\boldsymbol{\mathcal{E}}} = \alpha \overline{\boldsymbol{B}} - \eta_t \mu_0 \overline{\boldsymbol{J}}. \qquad (3)$$

The coefficients linking correlations to mean quantities are known unimaginatively as mean-field transport coefficients, with each one describing a distinct physical effect. In equation (3), α describes the (in)famous α effect that can drive a dynamo, while η_t quantifies the turbulent diffusion of the mean magnetic field (μ_0 is the vacuum permeability). Note that a much more general representation of $\overline{\boldsymbol{\mathcal{E}}}$ is given by the convolution integral

$$\overline{\boldsymbol{\mathcal{E}}}(\boldsymbol{x}, t) = \int_{t_0}^{t} \int \boldsymbol{G}(\boldsymbol{x}, \boldsymbol{x}', t, t')\, \overline{\boldsymbol{B}}(\boldsymbol{x}', t')\, \mathrm{d}^3 x'\, \mathrm{d}t' \qquad (4)$$

with an appropriate tensorial kernel $\boldsymbol{G}$.

Equation (2) contains terms that can sometimes be neglected. Most famously, in the case of fluids with small magnetic Reynolds number, that is $Re_{\mathrm{M}} = UL/\eta \ll 1$, or low Strouhal number $St = U\tau_c/L \ll 1$, we can drop $(\boldsymbol{u} \times \boldsymbol{b})'$ and can thus make an analytical calculation of the transport coefficients feasible. Under this approximation, known as the second order correlation approximation (SOCA), equation (2) takes for vanishing mean velocity the form

$$\frac{\partial \boldsymbol{b}}{\partial t} = \nabla \times \left(\boldsymbol{u} \times \overline{\boldsymbol{B}} \right) + \eta \nabla^2 \boldsymbol{b}. \qquad (5)$$

In the limit of high Re_{M} (hence small St), the coefficients α and η_t reduce then to (Krause and Rädler 1980, Rädler and Rheinhardt 2007)

$$\alpha = -\frac{\tau_c}{3} \overline{\boldsymbol{u} \cdot (\nabla \times \boldsymbol{u})}, \quad \eta_t = \frac{\tau_c}{3} \overline{\boldsymbol{u}^2}, \qquad (6)$$

where τ_c is a characteristic turbulent correlation time.

2. The need for MFT: a status report

2.1. Motivation

In the astrophysical context, MFT has mainly been applied in order to understand and model the origin of the Sun's magnetic field and its differential rotation (Rüdiger and Hollerbach 2004). Direct simulations of convection in spherical shells begin to reproduce these phenomena to some extent (Brun *et al* 2004, Browning *et al* 2006, Brown *et al* 2010, Käpylä *et al* 2010a), but interpreting their results properly remains difficult. This task is approachable only in the framework of a reasonably accurate theory.

MFT is sometimes perceived as uncertain and even arbitrary owing to a large amount of parameters that are often chosen to reproduce 'whatever one wants'. Adjusting parameters at will is certainly risky and clearly not permissible in the long run, because it would imply a complete loss

of predictive power of MFT. There are several reasons why the 'free parameter' approach has nevertheless often been adopted. Firstly, the conventional theory for computing turbulent transport coefficients is only accurate at low Reynolds numbers, but is not well tested at higher ones. Secondly, models of solar-like dynamos that are based on a straightforward application of mixing-length ideas to computing turbulent transport coefficients (Krivodubskii 1984) do not reproduce the Sun: the cycle periods are too short (Köhler 1973) and the migration of sunspots and other magnetic activity is poleward, not equatorward, which is also found in direct numerical simulations (Gilman 1983, Käpylä *et al* 2010a).

In this situation, it is sensible to reduce one's ambitions and focus on phenomena that are seen in direct simulations of simplified systems, but are nevertheless relevant for understanding the Sun. A useful goal consists then in reproducing such phenomena by mean-field models, thus obtaining a chance to trace down the reasons for discrepancies between both representations. This will be exemplified in section 3. First, however, we shall summarize the basic saturation phenomenology of mean-field dynamos.

2.2. Saturated dynamos and magnetic helicity fluxes

A recent discovery that is now well explained by MFT is the slow saturation behavior of an α^2 dynamo in a triply periodic box (Brandenburg 2001). Such systems are unphysical, but they make good test problems due to the ease of capturing them both numerically and analytically. Initially, both the mean and the fluctuating fields grow exponentially—as expected from kinematic theory. However, when the small-scale field becomes comparable to the equipartition value, i.e. $\overline{\boldsymbol{b}^2} \sim B_{\mathrm{eq}}^2$, the growth changes its nature: the fluctuating field saturates while the mean field, well below equipartition, continues to grow albeit extremely slowly. Finally, after multiple microphysical resistive times, the mean field itself reaches a steady, super-equipartition state; see figure 9.4 of Brandenburg and Subramanian (2005).

This behavior is one aspect of the 'catastrophic' α-quenching phenomenon, and has come to be understood in terms of the magnetic helicity density, $h \equiv \boldsymbol{A} \cdot \boldsymbol{B}$, and the magnetic α effect of Pouquet *et al* (1976), $\alpha_{\mathrm{M}} \equiv \tau \overline{\boldsymbol{j} \cdot \boldsymbol{b}}/3\overline{\rho}$. It has usually the opposite sign of the α of equation (6), now marked α_{K} (kinetic), and grows with growing mean field, so that the net $\alpha = \alpha_{\mathrm{K}} + \alpha_{\mathrm{M}}$ would be reduced and the dynamo growth halted. This result has been extended to the dynamic α quenching phenomenology (Kleeorin and Ruzmaikin 1982, Field and Blackman 2002, Blackman and Brandenburg 2002), where the mean magnetic helicity in the fluctuating fields, $h_{\mathrm{f}} \equiv \overline{\boldsymbol{a} \cdot \boldsymbol{b}}$, is used as a proxy for the current helicity, $\overline{\boldsymbol{j} \cdot \boldsymbol{b}} \simeq k_{\mathrm{f}}^2 h_{\mathrm{f}}$, with k_{f} being the wavenumber of the energy-carrying eddies. In a system that disallows the divergence of the magnetic helicity flux, such as a triply periodic domain, the time evolution of h_{f} and the resulting dynamical α quenching equation can be written as

$$\frac{\mathrm{d}h_{\mathrm{f}}}{\mathrm{d}t} = -2\overline{\boldsymbol{\mathcal{E}}} \cdot \overline{\boldsymbol{B}} - 2\eta \mu_0 \overline{\boldsymbol{j} \cdot \boldsymbol{b}}, \qquad (7)$$

$$\frac{\mathrm{d}\alpha_\mathrm{M}}{\mathrm{d}t} = -2\eta_t k_\mathrm{f}^2 \left(\frac{\alpha \overline{B}^2 - \eta_t \mu_0 \overline{J} \cdot \overline{B}}{B_\mathrm{eq}^2} + \frac{\alpha_\mathrm{M}}{Re_\mathrm{M}} \right). \qquad (8)$$

The three phases of the α^2 dynamo in a triply periodic domain can now be understood. First the fields grow exponentially and the magnetic α effect grows with them until $\alpha_\mathrm{M} \sim -\alpha_\mathrm{K}$. This occurs rapidly enough that the magnetic helicity of the mean field (h_m) still obeys $h_\mathrm{m} \sim -h_\mathrm{f}$ and so $\overline{B}/B_\mathrm{eq} \simeq \sqrt{k_1/k_\mathrm{f}} < 1$ (Brandenburg 2001), where k_1 is the smallest possible wavenumber in the domain. During the resistive phase, the fluctuating fields are nearly steady but there is still a small excess of α over $\eta_t k_1$ needed to replenish the field in the face of resistivity. This phase ends only when the time evolution of the total magnetic helicity reaches a steady state, which occurs when $\langle \boldsymbol{J} \cdot \boldsymbol{B} \rangle = 0$ or $\overline{B}/B_\mathrm{eq} \simeq \sqrt{k_\mathrm{f}/k_1} > 1$.

A short exponential growth phase yielding only weak mean fields poses severe problems for astrophysics as the subsequent resistive growth phase is generally prohibitively long. Real systems, however, allow for fluxes of magnetic helicity across their borders, and/or show spatial variations in the α effect, particularly regions where α has opposite signs separated, say, by an equator. This raises the possibility that the magnetic α will be exported from the system or transported to the equator and destroyed. Research into such transport is recent, but has already shown conclusively that there is a flux of h_f and that a larger residual α effect results due to it. It is not yet clear how large an effect this has on the final mean field strength.

3. Predictions versus realizations

In this section, we contrast the results of some computer realizations with corresponding mean-field predictions. We discuss examples from both linear and nonlinear regimes.

3.1. Parity and dependence on boundary conditions

A relatively old example is the emergence of oscillatory dynamo solutions in local models of accretion discs (Brandenburg *et al* 1995). Here, turbulence is driven by the magneto-rotational instability that generates a negative α effect in the upper half of the disc (Brandenburg *et al* 1995, Ziegler and Rüdiger 2000, Brandenburg 2005a, Gressel 2010). According to MFT, this negative α, for normal field (pseudo-vacuum) boundary conditions and radial shear, results in traveling wave solutions that are symmetric about the midplane and migrating toward the boundaries (Brandenburg and Campbell 1997). Conversely, when the boundary condition is changed to a perfect conductor, one expects non-oscillatory solutions that are antisymmetric about the midplane. Indeed, this dependence is borne out by simulations (Brandenburg 1998).

3.2. Onset of convective dynamo action depending on rotation rate

Large-scale dynamos due to turbulent convection are of particular interest in astrophysics. According to MFT, rotating inhomogeneous (usually due to stratification) turbulence leads to the generation of kinetic helicity and thus an α effect, which

should enable the generation of large-scale fields. However, numerical simulations of rotating convection at first failed to show large-scale dynamo action (e.g. Brandenburg *et al* 1996, Cattaneo and Hughes 2006). Erroneously low values of α determined by what is now often called the imposed-field method seemed to confirm that the α effect does not work. In this method, a uniform magnetic field $\boldsymbol{B}_0$ is applied and one determines the resulting mean electromotive force, $\langle \boldsymbol{u} \times \boldsymbol{b} \rangle$, and further $\alpha = \langle \boldsymbol{u} \times \boldsymbol{b} \rangle \cdot \boldsymbol{B}_0/B_0^2$; here the mean is defined as volume average (e.g. Cattaneo and Hughes 2006; see, however, Käpylä *et al* 2010b). On the other hand, when computing the turbulent transport coefficients for convection using the test-field method (see section 4.1), it was discovered that, as the rotation rate in non-shearing runs increases, the α effect increases and turbulent diffusion, η_t, decreases (Käpylä *et al* 2009a). Mean-field models (hereafter MFM), using these properly determined transport coefficients, then suggested that a large-scale dynamo should be excited when the Coriolis number, defined as the ratio of the rotation period to the convective turnover time, exceeds a value of ≈ 4. Subsequently, direct simulations in this parameter range confirmed this prediction (Käpylä *et al* 2009b). Again, this demonstrates that already kinematic MFT has predictive power and that very likely MFMs can give useful and new information about even more complex systems.

3.3. Helicity considerations

The helicity considerations outlined in section 2.2 provide further prognostic power. The shear-induced (non-diffusive) magnetic helicity flux, introduced by Vishniac and Cho (2001), has been particularly important in explaining the existence or the absence of a large-scale dynamo. For example, Tobias *et al* (2008) presented simulations of convection with vertical shear where no large-scale dynamo was excited although the necessary ingredients for an efficient dynamo (inhomogeneity, rotation and shear) were all present. However, in that case the shear-driven magnetic helicity flux is directed along the periodic x-direction and no net flux out of the system could occur. Using instead, in an otherwise similar setup, normal field boundary conditions, which do allow a net flux, Käpylä *et al* (2008) showed that a large-scale dynamo does exist and indeed saturates at near-equipartition field strengths; see the left panel of figure 1 where we show the effect of open versus periodic boundaries. Similar results have also been obtained for forced turbulence with a more complicated shear profile motivated by the differential rotation pattern of the Sun (Brandenburg 2005b). By imposing a toroidal magnetic field in a simulation with the same setup, the α effect has been determined and, for $Re_\mathrm{M} \gg 1$, it is also found to depend sensitively on whether the boundaries are open or closed (Brandenburg and Sandin 2004); see the right panel of figure 1.

Another issue approachable through magnetic helicity considerations is the convergence problem of the MRI, i.e. the steep decrease of the turbulence level with decreasing magnetic Prandtl number, Pr_M, for small values of Pr_M in fully periodic setups (e.g. Fromang *et al* 2007). An otherwise similar setup, however, that does allow a net magnetic helicity flux through the vertical boundaries produces indeed strong
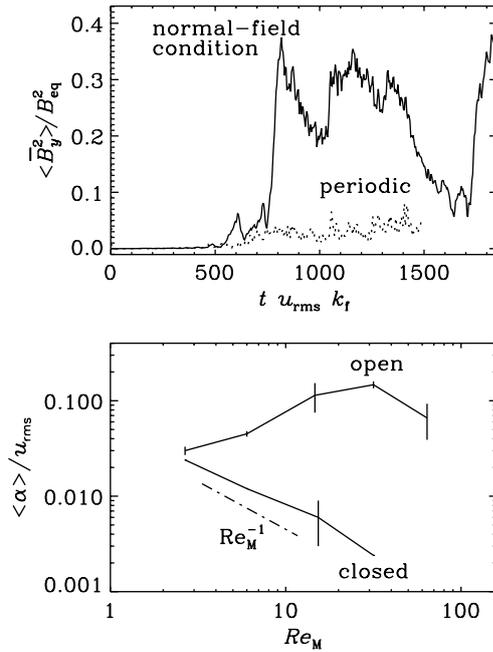
Figure 1. Upper plot: energy in the horizontally averaged streamwise magnetic field from two convection simulations with vertical shear $\overline{U}_y(z)$ and either normal field (solid line) or periodic (dotted line) magnetic boundary conditions in the x-direction. Adapted from Käpylä *et al* (2008). Lower plot: dependence of $\langle\alpha\rangle/u_{\rm rms}$ on $Re_{\rm M}$ for open and closed boundaries. Note that for $Re_{\rm M} \approx 30$ the α effect is about 30 times smaller when the boundaries are closed. Adapted from Brandenburg and Sandin (2004).

large-scale dynamo action, roughly independent of the value of $Pr_{\rm M}$ (Käpylä and Korpi 2010).

4. Computing mean-field transport coefficients

In view of such success stories, there should be an unbroken interest in MFMs both because of their descriptive capabilities and their predictive potential, but we have to realize that there are serious shortcomings of MFT that have persuaded many researchers to (re)turn to global direct numerical simulations instead of designing improved MFMs. This critical stage of MFT can be characterized by the following observations:

- The limitations of analytic approaches to calculating mean-field coefficients are clearly too restrictive as the interest has moved from pointing out the qualitative existence of certain effects to their quantitative reproduction and prediction. This is due to
  * the obvious insufficiency of SOCA in astrophysical contexts, as usually $Re_{\rm M} \gg 1$ and $St \ll 1$;
  * the unclear aspects of closure approaches like the τ approximation (Rädler and Rheinhardt 2007);
  * the need for knowledge of velocity correlators like $\overline{u_i u_j \cdots u_n}$ even in mathematically well-established (systematic) higher-order correlation approximations.
- It is obvious that MFMs for realistic setups with predictive abilities need to employ transport coefficients that are
  * fully tensorial;
  * position dependent;

  * dependent on the mean quantities themselves, i.e. nonlinear;
  * non-local and non-instantaneous;
  * including magnetic background fluctuations.

  There is no longer any chance of obtaining powerful models by employing a few scalar coefficients, the basic structure of which can be derived analytically leaving a few free parameters to be adapted properly.

To find a way out of this impasse, one might look at how in other fields of physics/engineering, modeling and simulation of rather complex systems are being made possible if the full resolution of the microphysics is not affordable. Let us choose as an example the mechanics of elastic materials, say, metals. Their elastic properties can in principle be derived from the microphysics of their lattices, but it will perhaps never be possible to simulate the static and dynamic behavior of, say, a bridge by solving quantum physical lattice equations. Instead, one relies upon the equations of continuum mechanics in which the lattice physics enters via macrophysical material properties such as Young's modulus and the Poisson number (sufficient for an isotropic material). These are typically obtained by measurements in a series of standardized experiments with test bodies having simple geometries and being subject to clearly defined boundary conditions. Of course, for such an approach to be successful, a certain *locality* of the microphysics processes is necessary, which can be expressed by the principle that neighboring material elements of a structure 'communicate' only via forces at their common borders.

A widely analogous procedure with respect to the task of calculating transport coefficients for a certain type of turbulence would consist in creating it in a (small) test volume with well-defined boundary/environmental conditions (such as a penetrating magnetic and/or gravitational field) and to determine then the wanted coefficients somehow *by measurements*. Then a major theoretical challenge consists in specifying the set of experiments needed to find just these coefficients and in prescribing the computational recipe for extracting them from the measured quantities such as fluctuating magnetic fields and/or velocities.

This program has been implemented by the so-called *test-field methods* (Schrinner *et al* 2005, 2007) with the modification that the physical experiments are replaced by numerical ones. Clearly, there is an important difference compared to the continuum mechanics scheme: the same equations whose direct simulation was felt to be non-affordable, what just created the need for an MFM, have now, nevertheless, to be simulated within the numerical experiments. However, in two aspects the test-field approach can still be advantageous. Firstly, the 'experimental' volumes can represent small sections of the object that is to be globally analyzed. Hence, much finer structures can be resolved with the same numerical effort. Secondly, if an MFM is established once, it can thereafter be utilized for long-term global simulations, which would otherwise be prohibitively expensive.

The aforementioned locality of the actual physics here has to be with respect to correlation properties of the underlying fluctuating fields, say, a turbulent flow. For all conceivable astrophysical situations this condition can hardly

be considered too restrictive. In practice, correlation lengths and times are the relevant quantities to be considered in defining the simulation box size and the integration time.

Computing turbulent transport tensors such as $\boldsymbol{\alpha}$ and $\boldsymbol{\eta}$ (see equation (9) below) from simulations has been performed with varying success over the last 20 years. Utilizing the imposed-field method for $\boldsymbol{\alpha}$ has led to either the confirmation of well-known results (for example, a positive horizontal α effect in the upper layers of convection in the Sun's Northern hemisphere) or the prediction of as yet unknown results (e.g. a reversed sign of the vertical α under the same conditions; see Brandenburg *et al* 1990) later confirmed by analytical calculations (Ferrière 1992, Rüdiger and Kitchatinov 1993).

After having explained the new test-field method in the next section, particular applications considering the nonlocality of turbulent transport in space and time will be discussed in section 4.2.

4.1. Test-field method

Let us return to equation (2) for the fluctuating magnetic field. The wanted mean electromotive force $\overline{\boldsymbol{\mathcal{E}}} = \overline{\boldsymbol{u} \times \boldsymbol{b}}$ is obviously a linear and homogeneous functional of $\overline{\boldsymbol{B}}$ and we may therefore write the ansatz

$$\overline{\boldsymbol{\mathcal{E}}} = \boldsymbol{\alpha}\overline{\boldsymbol{B}} - \boldsymbol{\eta}\nabla\overline{\boldsymbol{B}}, \qquad (9)$$

strictly valid for stationary mean fields depending only linearly on position. The components of $\boldsymbol{\alpha}$ and $\boldsymbol{\eta}$ can be found by the following procedure:

(a) solve

$$\frac{\partial \boldsymbol{b}^k}{\partial t} - \eta\nabla^2\boldsymbol{b}^k - \mathrm{curl}\left[(\overline{\boldsymbol{U}} \times \boldsymbol{b}^k + \boldsymbol{u} \times \boldsymbol{b}^k)'\right] = \mathrm{curl}\,(\boldsymbol{u} \times \overline{\boldsymbol{B}}^k)$$

for given $\boldsymbol{u}, \overline{\boldsymbol{U}}$ and test fields $\overline{\boldsymbol{B}}^k$, $k = 1, \ldots, N$;

(b) calculate $\overline{\boldsymbol{\mathcal{E}}}^k = \overline{\boldsymbol{u} \times \boldsymbol{b}^k}$;

(c) determine the components of $\boldsymbol{\alpha}$ and $\boldsymbol{\eta}$ by inverting

$$\overline{\boldsymbol{\mathcal{E}}}^k = \boldsymbol{\alpha}\overline{\boldsymbol{B}}^k - \boldsymbol{\eta}\nabla\overline{\boldsymbol{B}}^k. \qquad (10)$$

The solution is unique if N is chosen appropriately and the test fields $\overline{\boldsymbol{B}}^k$ are sufficiently independent. Since we 'look at' the given velocity fields $\boldsymbol{u}, \overline{\boldsymbol{U}}$ not from only one perspective like in the case of the imposed-field method, but obtain instead different views represented by the different test solutions $\boldsymbol{b}^k$, the test-field approach could be characterized as 'holographic' instead of 'photographic'. Indeed, all of the information needed to specify an ansatz like (9) is extracted from the velocity fields.

For a number of explicitly given flows like those introduced by Roberts (1970) and Galloway and Proctor (1992), exact agreement of the determined tensors with SOCA results could be demonstrated. In the case of the Roberts flow there is agreement even with an analytic result for arbitrary magnetic Reynolds numbers (Rädler *et al* 2002, Rädler and Brandenburg 2009, Rheinhardt and Brandenburg 2010).

The method has now been applied to a number of different flows ranging from homogeneous forced turbulence without shear (Sur *et al* 2008, Brandenburg *et al* 2008a) to cases with shear (Brandenburg *et al* 2008b, Mitra *et al*

2009) and to inhomogeneous turbulence in stratified discs (Brandenburg 2005a, Gressel *et al* 2008) as well as convection (Käpylä *et al* 2009a). It has also been utilized in passive scalar transport, e.g. the transport of chemicals. Corresponding turbulent transport coefficients have been calculated for homogeneous turbulence under the influence of rotation or an applied magnetic field (Brandenburg *et al* 2009), as well as for homogeneous shear flows (Madarassy and Brandenburg 2010).

4.2. Nonlocality in space and time

Because the test fields are not native to the system, they can disentangle effects that can not otherwise be distinguished. However, for the same reason they can introduce temporal or spatial scales that are again not native to the system.

With respect to temporal scales the consequences of this mismatch can be seen in the *memory effect*: consider a dynamo system with a growing mean field. Turbulence creates a fluctuating field from the mean one and contributes to the mean electromotive force. If the mean field is growing, the small-scale field created in the past is weaker than it would be when created in the present. Thus, if the time behavior of the test fields is different from that of the 'real' mean field, the $\boldsymbol{\alpha}$ and $\boldsymbol{\eta}$ tensors from the test-field method will not be the actual ones that rule the evolution of the mean field. A similar problem occurs when the spatial scales of the test fields do not coincide with the spatial scale of the mean field to be modeled, due to *nonlocality* in space.

When the proper scales of the mean field are known, corresponding test fields can be used. Otherwise, the scales of the test fields, say, wavevector $\boldsymbol{k}$ and frequency ω, are considered independent parameters and the test-field method provides $\boldsymbol{\alpha}(\boldsymbol{k}, \omega)$ and $\boldsymbol{\eta}(\boldsymbol{k}, \omega)$, which exhaustively describe the response kernel introduced in (4).

The memory effect is demonstrated in figure 2 for the case of the Roberts flow (for details, see Hubbard and Brandenburg (2009). In the left plot, we see the difference between the growth rate of a dynamo and that calculated from the dispersion relation using $\boldsymbol{\alpha}$ and $\boldsymbol{\eta}$ determined by the test-field method with steady test fields. We can reconcile these growth rates by deriving them all from a proper kernel, which can be established by employing a set of test fields with different time dependences.

The memory effect and nonlocality in space have been studied using the integral kernel technique in Hubbard and Brandenburg (2009) and Brandenburg *et al* (2008a), respectively. Using test fields that oscillate sinusoidally in time, the Fourier transforms $\hat{\alpha}(\omega)$ of the integral kernels $\tilde{\alpha}(t)$ were found to fit the form:

$$\hat{\alpha}(\omega) = \alpha_0 \frac{1 - \mathrm{i}\omega\tau_\alpha}{(1 - \mathrm{i}\omega\tau_\alpha)^2 + \omega_\alpha^2\tau_\alpha^2}, \qquad (11)$$

where τ_α is the memory time of the flow and ω_α is a fit parameter of order τ_α^{-1}. In turbulence, τ_α is comparable to the turnover time, but in steady flows, it can approach microphysical resistive time scales. In the right panel of figure 2, we present such a fit for the MW + flow of Otani (1993), being a flow pattern with wavenumber k_0 and amplitude u_0 that is modulated with frequency $\omega_\mathrm{f} = u_0 k_0$.
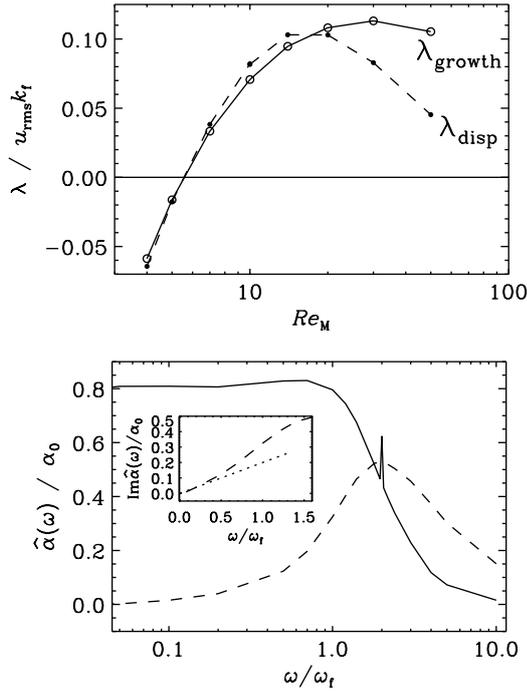
Figure 2. Upper plot: Re_M dependence of the dynamo growth rate for the Roberts flow as obtained from a direct calculation, $\lambda_{\mathrm{growth}}$, compared with the result of the dispersion relation, $\lambda_{\mathrm{disp}} = |\alpha k| - (\eta + \eta_t)k^2$, using a cube of size L^3; $k_1 = 2\pi/L$, $k_f = \sqrt{2}k_1$. For this range of Re_M, the most unstable mode has the largest possible wavelength ($k = k_1$). Lower plot: real (solid) and imaginary (dashed) parts of $\hat{\alpha}(\omega)$ for $k = 0$ using the Otani (1993) MW+ flow with $Re_M = 1$. Normalization given by $\alpha_0 = u_0$. Inset: scaling of Im $\hat{\alpha}$ near the origin with slope 0.2, in agreement with the results of Hughes and Proctor (2010). Adapted from Hubbard and Brandenburg (2009).

This leads to an extra spike in $\hat{\alpha}(\omega)$ at $\omega = 2\omega_f$. The slope of the imaginary part at the origin, $\mathrm{dIm}\,\hat{\alpha}/\mathrm{d}\omega|_{\omega=0}$, represents the coefficient of the first order term with respect to an expansion in time. Its value of 0.2 is in agreement with that found by Hughes and Proctor (2010). The real-space integral kernel corresponding to (11) reads

$$\tilde{\alpha}(\tau) = \alpha_0 \Theta(\tau) e^{-\tau/\tau_\alpha} \cos \omega_\alpha \tau, \qquad (12)$$

where τ is the time distance to the instant of consideration, and Θ is the Heaviside step function that preserves causality as the time integral kernel must only consider the past. Hubbard and Brandenburg (2009) have found similar expressions also for passive scalar transport.

The Fourier transform of the spatial integral kernels is somewhat simpler, being fit by a Lorentzian:

$$\hat{\alpha}(k) = \frac{\alpha_0}{1 + (a_\alpha k/k_f)^2}, \qquad \hat{\eta}_t(k) = \frac{\eta_{t0}}{1 + (a_\eta k/k_f)^2}, \quad (13)$$

whose amplitude is nearly independent of Re_M for $Re_M \gg 1$. The k dependence is reasonably close to inverse quadratic for $k/k_f > 2$; see figure 3. Here, $a_\alpha \approx 2a_\eta \approx 1$ are coefficients of the order of unity. The corresponding spatial integral kernels are simple exponential decays

$$\tilde{\alpha}(\zeta) = \alpha_0 \frac{k_f}{2a_\alpha} e^{-(k_f/a_\alpha)\zeta}, \qquad \tilde{\eta}_t(\zeta) = \eta_{t0} \frac{k_f}{2a_\eta} e^{-(k_f/a_\eta)\zeta}, \qquad (14)$$

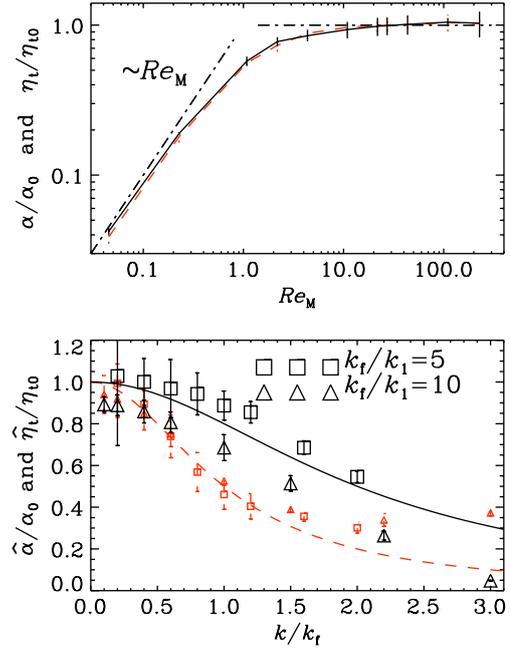where ζ is the distance from the point of consideration.

Figure 3. Upper plot: dependence of the normalized values of α (dashed or red line) and η_t (solid line) on Re_M for $k/k_f = 0.2$ and $Re = 2.2$. Adapted from Sur *et al* (2008). Lower plot: dependences of the normalized $\hat{\alpha}$ (dashed or red line, small symbols) and $\hat{\eta}_t$ (solid line, bigger symbols) on the normalized wavenumber k/k_f for turbulence forced with $k_f/k_1 = 5$, $Re_M = 10$ (squares) and $k_f/k_1 = 10$, $Re_M = 3.5$ (triangles). Lines give the Lorentzian fits (13). Adapted from Brandenburg *et al* (2008a).

5. From linear to nonlinear

When the velocity U is given, the tensors α and η can be obtained by a mathematically well-founded procedure as outlined in section 4.1. Naturally, the question arises as to how one should proceed when the mean magnetic field has already acted upon this velocity. Inspecting equation (2) it can be concluded that $\overline{B}$, considered as a functional of U and $\overline{B}$, is always linear and homogeneous in the latter, irrespective of the effects that U was subjected to and, in particular, irrespective of whether or not a mean field had already acted upon it. That is, the presented test-field method continues to be valid without modification and as a tribute to this extension it is called the *quasi-kinematic method*. The turbulent transport coefficients are of course now depending on $\overline{B}$, but this dependence is entirely conveyed by the dependence of U on $\overline{B}$.

Clearly, a dynamically effective mean field represents an additional preferred direction. As a consequence, for an isotropic hydrodynamic background and a uniform $\overline{B}$, the formerly isotropic tensor α adopts now the shape

$$\alpha_{ij} = \alpha_1 \delta_{ij} + \alpha_2 \hat{B}_i \hat{B}_j, \quad i, j = 1, 2, \qquad (15)$$

with $\hat{B}$ being the unit vector in the direction of $\overline{B}$. If this is, say, the x-direction we get $\alpha_{11} = \alpha_1 + \alpha_2$ and $\alpha_{22} = \alpha_1$. Both coefficients are of course functions of $\overline{B}$. Since $\overline{\mathcal{E}} = \alpha_{11}\overline{B}$, the effective scalar α effect is just given by α_{11}. As an example, the α quenching characteristic for the Roberts flow was determined exhibiting a $\overline{B}^{-4}$ asymptotic dependency, cf Rheinhardt and Brandenburg (2010) and figure 4. This
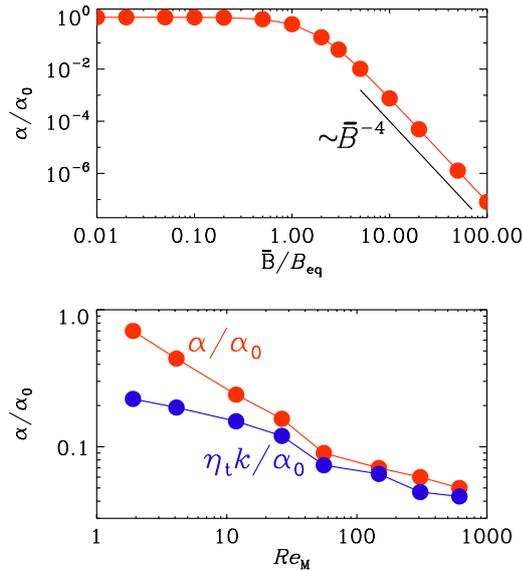
Figure 4. Upper plot: variation of α with $\overline{B}$ for the forced Roberts flow with $Re_{\rm M} = 1/2\sqrt{2} \approx 0.35$ and $Pr_{\rm M} = 1$. Adapted from Rheinhardt and Brandenburg (2010). Lower plot: $Re_{\rm M}$ dependence of α and $\eta_{\rm t}$ in the saturated state with $\overline{B} \approx B_{\rm eq}$. Adapted from Brandenburg *et al* (2008c).

result is at odds with theoretical predictions, although it agrees with data for a forced ABC flow (Sur *et al* 2007).

Things become more involved if the direction of the mean current density $\overline{J}$ enters as a second preferred direction. A situation in which this complication is circumvented, without being as simple as the former one, is given by the α^2 dynamo due to homogeneous isotropic helical (forced) turbulence. Here, the dynamo solution is a Beltrami field with $\overline{B} \parallel \overline{J}$ and constant modulus. Hence, $\overline{J}$ is not providing an additional preferred direction and equation (15) remains valid. The solution has always Beltrami shape, regardless of at what level it eventually saturates. Consequently, α and $\eta_{\rm t}$ are independent of position for any field strength. The growth rate of the dynamo is given by $\lambda = |\alpha k| - (\eta + \eta_{\rm t})k^2$ and should approach zero in the course of saturation. Under these conditions it is possible to confirm the quasi-kinematic method in the way that $\alpha(\overline{B})$and $\eta_{\rm t}(\overline{B})$ are determined in the saturated stage and checked for consistency against $\lambda = 0$. Indeed, this could be demonstrated to high accuracy for different values of $Re_{\rm M}$; see Brandenburg *et al* (2008c). Figure 4 shows $\alpha(\overline{B})$ and $\eta_{\rm t}(\overline{B})$ as functions of $Re_{\rm M}$ in the saturated state with $\overline{B} \approx B_{\rm eq}$.

6. Quasi-kinematic method for magnetic-buoyancy-driven flows

So far, we have been dealing with situations in which a hydrodynamic background was provided independently and the mean magnetic field occurred as an additional, at most coequal participant. But what about cases in which the turbulence itself is a consequence of $\overline{B}$? Examples are the magneto-rotational instability and the magnetic buoyancy instability (see below). Clearly, those setups do not know a kinematic stage on which the influence of $\overline{B}$ is negligible. One might worry that in such a situation the quasi-kinematic

test-field procedure fails (Courvoisier *et al* 2010). However, equation (2) continues to be valid and hence all conclusions drawn from it. Consequently, the quasi-kinematic method should be applicable. The only peculiarity occurring here is the fact that all components of $\boldsymbol{\alpha}$ and $\boldsymbol{\eta}$ vanish for $0 \leqslant \overline{B} \leqslant \overline{B}_{\rm threshold}$, because a fluctuating velocity (and magnetic field) develops only after the instabilities have set in.

Let us now consider the magnetic buoyancy instability. It has been proposed by Moffatt (1978) that, once the dynamo-generated magnetic field in the overshoot layer of the Sun reaches appreciable strengths, this instability can set in and govern the dynamics thereafter. The buoyancy instability of a localized flux layer in the presence of stratification and rotation was later studied in detail by Schmitt (1984, 1985). A necessary but not sufficient condition for instability is

$$\frac{\partial}{\partial z} \log\left(\frac{B^2}{\rho^2}\right) < 0, \qquad (16)$$

which essentially means that the magnetic field decreases faster with height than density. Using the imposed-field method, Brandenburg and Schmitt (1998) performed numerical calculations to determine the α effect of the resulting turbulence. Here we determine all components of $\boldsymbol{\alpha}$ and $\boldsymbol{\eta}$ using a version of the quasi-kinematic test-field method wherein mean fields are defined as xy averages.

Our setup is similar to that described in Brandenburg and Schmitt (1998). The computational domain is a cuboid of size $-1 \leqslant x \leqslant 1$, $-3 \leqslant y \leqslant 3$, $-0.5 \leqslant z \leqslant 1.5$, with gravity pointing in the negative z-direction, and rotation $\boldsymbol{\Omega}$ making an angle θ with the vertical. The pressure scale height is $H_{\rm P} = 1$ (half-height of the box). The base state is a polytrope with index $m = 3$ (the adiabatic value here is $3/2$), so that it is stable to convection. The initial condition comprises a horizontal magnetic layer of thickness $H_{\rm B} = 0.1$ with the profile

$$B_y = v_{\rm A0} H_{\rm B} \frac{\partial}{\partial z} \tanh\left(\frac{z - 0.1}{H_{\rm B}}\right), \qquad (17)$$

where the ratio of the reference values of Alfvén and sound speed is $v_{\rm A0}/c_{\rm s0} = 0.5$. We modify the base state such that the density profile remains polytropic but the entropy profile is adjusted to obey magnetostatic equilibrium. The initial velocity consists of about 20 localized eddies with Mach numbers of about 10^{-5} at $z = 0.1$ in the xy-plane. We use stress-free boundary conditions for the velocity and the vertical field condition for the magnetic field, whereas with respect to entropy we keep the temperature at the top and the (radiative) heat flux at the bottom constant. All calculations have been done with $Pr = Pr_{\rm M} = 4$ on a 64^3 grid. Figure 5(a) gives the temporal evolution of the volume averages $\langle u^2 \rangle$ and $\langle B_x^2 \rangle$ and figure 5(b) the evolution of the mean field $\overline{B}_x$. There is a short exponential growth phase followed by a slow decay on a resistive time scale.

When it comes to applying the test-field method, an aspect not discussed up to now is the intrinsic inhomogeneity of the flow both due to stratification and the background magnetic field itself. Within kinematics, that is, without the background field, no specific complication is connected to this, as from the stationary version of equation (4),
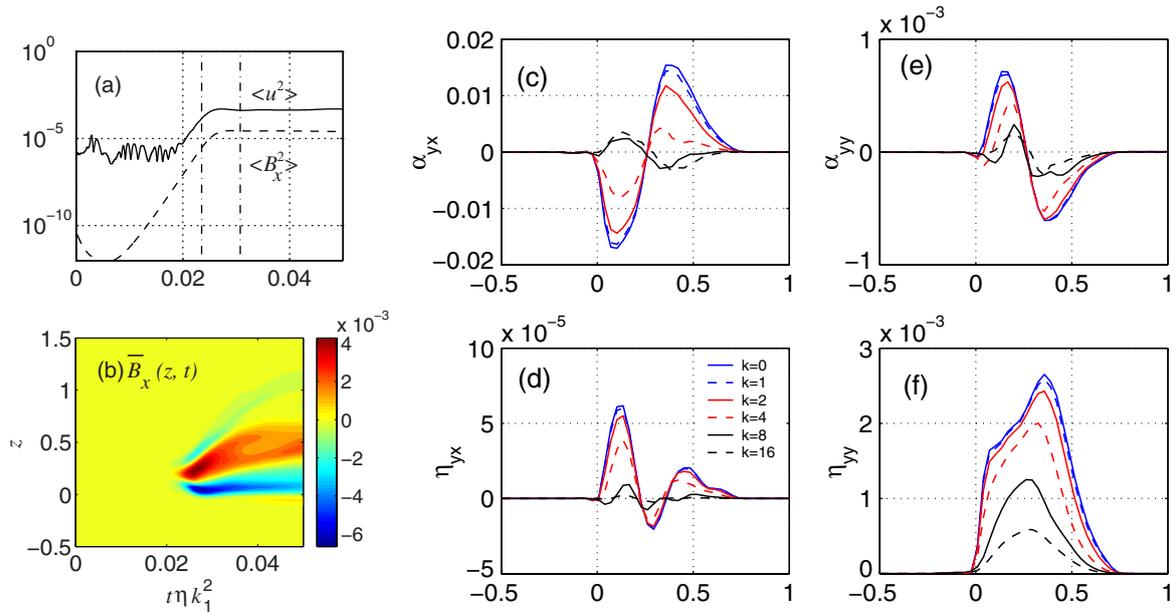
Figure 5. (a) Evolution of volume averaged velocity and B_x squares. (b) A 'butterfly diagram' for $\overline{B}_x$. (c–f) Selected tensorial components of $\hat{\boldsymbol{\alpha}}$ and $\hat{\boldsymbol{\eta}}$ for different wavenumbers k as explained in the legend in (d). Plots have been obtained by time averaging over the interval indicated by the dashed-dotted lines in (a).
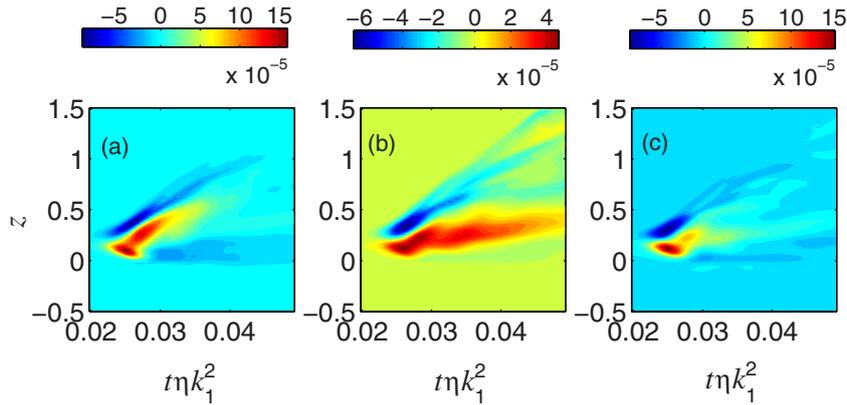

Figure 6. (a) The mean emf $\overline{\mathcal{E}}_y(z, t)$ calculated from the horizontal average $\overline{\boldsymbol{u} \times \boldsymbol{b}}$. (b) Reconstruction of $\overline{\mathcal{E}}_y(z, t)$ using only the $k = 0$ contributions in (18). (c) The same as (b) but using all contributions $k = 0, 1, \ldots 8$.

$\boldsymbol{\alpha}$ and $\boldsymbol{\eta}$ emerge straightforwardly in a shape expressing inhomogeneity, that is, $\boldsymbol{\alpha}(\boldsymbol{x}, \boldsymbol{x}')$, $\boldsymbol{\eta}(\boldsymbol{x}, \boldsymbol{x}')$ or, equivalently, $\boldsymbol{\alpha}(\boldsymbol{x}, \boldsymbol{x} - \boldsymbol{x}')$, $\boldsymbol{\eta}(\boldsymbol{x}, \boldsymbol{x} - \boldsymbol{x}')$. When subjecting the latter to a Fourier transform with respect to their second argument, we arrive at $\hat{\boldsymbol{\alpha}}(\boldsymbol{x}, \boldsymbol{k})$ and $\hat{\boldsymbol{\eta}}(\boldsymbol{x}, \boldsymbol{k})$. In our case, harmonic test fields with different wavenumbers k in the z-direction can be employed to obtain $\hat{\boldsymbol{\alpha}}(z, k)$ and $\hat{\boldsymbol{\eta}}(z, k)$.

In the nonlinear situation, the Green's function approach remains valid if $\overline{\mathcal{E}}$ is considered as a functional of $\boldsymbol{U}$ and $\overline{\boldsymbol{B}}$, which is then linear and homogeneous in the latter (cf section 5). However, we have to label $\boldsymbol{G}$ by the $\overline{\boldsymbol{B}}$ actually acting upon $\boldsymbol{U}$, that is, $\boldsymbol{G}(\boldsymbol{x}, \boldsymbol{x}'; \overline{\boldsymbol{B}})$, and can thus only make statements about the transport tensors for just the particular $\overline{\boldsymbol{B}}$ at hand. Hence, the tensors have to be labeled likewise: $\hat{\boldsymbol{\alpha}}(z, k; \overline{\boldsymbol{B}})$, $\hat{\boldsymbol{\eta}}(z, k; \overline{\boldsymbol{B}})$. As our initial mean magnetic field is in the y-direction, the instability will generate a $\overline{B}_x$ and we are mainly interested in the coefficients α_{yx}, α_{yy}, η_{yx} and η_{yy} with rank-2 tensor components $\eta_{ij} = -\eta_{ik3}\epsilon_{jk3}$; they are shown in figures 5(c)–(f). (Note that our rank-3 $\boldsymbol{\eta}$ tensor in

equation (9) is defined with the opposite sign as, for example, in Brandenburg *et al* (2008a).)

Our goal now is to confirm that the relationship between $\overline{\mathcal{E}}$ and $\overline{\boldsymbol{B}}$ taken directly from direct numerical simulations (DNS) can be represented by equation (9) with the transport tensors determined using the quasi-kinematic test-field method. In mathematical terms

$$\overline{\mathcal{E}}_i(z; \overline{\boldsymbol{B}}) \overset{?}{=} Re\left\{ \sum_k \left[\hat{\alpha}_{ij}(z, k; \overline{\boldsymbol{B}}) - i\pi k\, \hat{\eta}_{ij}(z, k; \overline{\boldsymbol{B}}) \right] \right.$$
$$\left. \times c_j^{(k)} \exp(i\pi k z) \right\}, \tag{18}$$

with $2c^{(k)} = \int \overline{\boldsymbol{B}}(z) \exp(-i\pi k z)\, dz$ and $\overset{?}{=}$ signifying the question whether the equation is indeed satisfied. We find that we can reasonably reconstruct the mean emf by truncating the infinite Fourier series already at $k = 8$. The result of the assembly of $\overline{\mathcal{E}}$ as formulated on the right-hand side of (18) is presented in figure 6(c) and turns out to be a

faithful reproduction of $\overline{\mathcal{E}}$ from the DNS shown in figure 6(a), especially during the exponential growth phase. We conclude that the quasi-kinematic test-field method may be used for correctly calculating transport coefficients even in the presence of inhomogeneous turbulence driven by an initial mean magnetic field.

7. Conclusions

MFT still has a lot to offer in terms of new effects and quantitative precision by combining analytics with numerics in parameter regimes that were previously inaccessible. The list of examples goes on and on; here we have only mentioned some of the most striking cases. The unmentioned ones concern, for example, the Reynolds and Maxwell stresses that have important applications in accretion discs (Blackman 2010) and possibly sunspot formation (Brandenburg *et al* 2010). Also of particular interest is the transport of passive scalars, admixed chemicals for example, as was mentioned briefly in section 4.1. The test-field method has been applied successfully to such cases as well. One may anticipate that all these aspects of MFT will soon grow in significance in our voyage toward understanding astrophysical dynamos.

Acknowledgments

References

Blackman E G 2010 *Astron. Nachr.* **331** 101
Blackman E G and Brandenburg A 2002 *Astrophys. J.* **579** 359
Brandenburg A 1998 *Theory of Black Hole Accretion Discs* ed M A Abramowicz, G Björnsson and J E Pringle (Cambridge: Cambridge University Press) p 61
Brandenburg A 2001 *Astrophys. J.* **50** 824
Brandenburg A 2005a *Astron. Nachr.* **326** 787
Brandenburg A 2005b *Astrophys. J.* **625** 539
Brandenburg A and Campbell C G 1997 *Accretion Disks—New Aspects* ed H Spruit and E Meyer-Hofmeister (New York: Springer) p 109
Brandenburg A and Sandin C 2004 *Astron. Astrophys.* **427** 13
Brandenburg A and Schmitt D 1998 *Astron. Astrophys.* **338** L55
Brandenburg A and Subramanian K 2005 *Phys. Rep.* **417** 1
Brandenburg A, Nordlund Å, Pulkkinen P, Stein R F and Tuominen I 1990 *Astron. Astrophys.* **232** 277
Brandenburg A, Nordlund Å, Stein R F and Torkelsson U 1995 *Astrophys. J.* **446** 741
Brandenburg A, Jennings R L, Nordlund Å, Rieutord M, Stein R F and Tuominen I 1996 *J. Fluid Mech.* **306** 325
Brandenburg A, Rädler K-H and Schrinner M 2008a *Astron. Astrophys.* **482** 739
Brandenburg A, Rädler K-H, Rheinhardt M and Käpylä P J 2008b *Astrophys. J.* **676** 740
Brandenburg A, Rädler K-H, Rheinhardt M and Subramanian K 2008c *Astrophys. J.* **687** L49
Brandenburg A, Svedin A and Vasil G M 2009 *Mon. Not. R. Astron. Soc.* **395** 1599
Brandenburg A, Kleeorin N and Rogachevskii I 2010 *Astron. Nachr.* **331** 5
Brown B P, Browning M K, Brun A S, Miesch M S and Toomre J 2010 *Astrophys. J.* **711** 424
Browning M K, Miesch M S, Brun A S and Toomre J 2006 *Astrophys. J.* **648** L157
Brun A S, Miesch M S and Toomre J 2004 *Astrophys. J.* **614** 1073
Cattaneo F and Hughes D W 2006 *J. Fluid Mech.* **553** 401
Courvoisier A, Hughes D W and Proctor M R E 2010 *Proc. R. Soc.* A **466** 583
Ferrière K 1992 *Astrophys. J.* **389** 286
Field G B and Blackman E G 2002 *Astrophys. J.* **572** 685
Fromang S, Papaloizou J, Lesur G and Heinemann T 2007 *Astron. Astrophys.* **476** 1123
Galloway D J and Proctor M R E 1992 *Nature* **356** 691
Gilman P A 1983 *Astrophys. J. Suppl.* **53** 243
Gressel O 2010 *Mon. Not. R. Astron. Soc.* **405** 41
Gressel O, Ziegler U, Elstner D and Rüdiger G 2008 *Astron. Nachr.* **329** 619
Hubbard A and Brandenburg A 2009 *Astrophys. J.* **706** 712
Hughes D W and Proctor M R E 2010 *Phys. Rev. Lett.* **104** 024503
Käpylä P J, Korpi M J and Brandenburg A 2008 *Astron. Astrophys.* **491** 353
Käpylä P J, Korpi M J and Brandenburg A 2009a *Astron. Astrophys.* **500** 633
Käpylä P J, Korpi M J and Brandenburg A 2009b *Astrophys. J.* **697** 1153
Käpylä P J, Korpi M J, Brandenburg A, Mitra D and Tavakol R 2010a *Astron. Nachr.* **331** 73
Käpylä P J, Korpi M J and Brandenburg A 2010b *Mon. Not. R. Astron. Soc.* **402** 1458
Käpylä P J and Korpi M J 2010 *Mon. Not. R. Astron. Soc.* submitted
Kleeorin N I and Ruzmaikin A A 1982 *Magnetohydrodynamics* **18** 116
Köhler H 1973 *Astron. Astrophys.* **25** 467
Krause F and Rädler K-H 1980 *Mean-Field Magnetohydrodynamics and Dynamo Theory* (Oxford: Pergamon)
Krivodubskii V N 1984 *Sov. Astron.* **28** 205
Larmor J 1919 *Rep. Br. Assoc. Adv. Sci.* 159
Madarassy E J M and Brandenburg A 2010 *Phys. Rev.* E **82** 016304
Mitra D, Käpylä P J, Tavakol R and Brandenburg A 2009 *Astron. Astrophys.* **495** 1
Moffatt H K 1978 *Magnetic Field Generation in Electrically Conducting Fluids* (Cambridge: Cambridge University Press)
Otani N F 1993 *J. Fluid Mech.* **253** 327
Parker E N 1955 *Astrophys. J.* **122** 293
Parker E N 1979 *Cosmical Magnetic Fields* (Oxford: Clarendon)
Pouquet A, Frisch U and Léorat J 1976 *J. Fluid Mech.* **77** 321
Rädler K-H and Brandenburg A 2009 *Mon. Not. R. Astron. Soc.* **393** 113
Rädler K-H and Rheinhardt M 2007 *Geophys. Astrophys. Fluid Dyn.* **101** 11
Rädler K-H, Rheinhardt M, Apstein E and Fuchs H 2002 *Magnetohydrodynamics* **38** 41
Rheinhardt M and Brandenburg A 2010 *Astron. Astrophys.* **520** A28
Roberts G O 1970 *Phil. Trans. Roy. Soc.* A **266** 535
Rüdiger G and Hollerbach R 2004 *The Magnetic Universe* (Weinheim: Wiley-VCH)
Rüdiger G and Kitchatinov L L 1993 *Astron. Astrophys.* **269** 581
Schmitt D 1984 *The Hydromagnetics of the Sun* ed T D Guyenne and J J Hunt (ESA N85-25091 14-92) p 223

Schmitt D 1985 Dynamowirkung magnetostrophischer Wellen *PhD Thesis* University of Göttingen

Schrinner M, Rädler K-H, Schmitt D, Rheinhardt M and Christensen U 2005 *Astron. Nachr.* **326** 245

Schrinner M, Rädler K-H, Schmitt D, Rheinhardt M and Christensen U R 2007 *Geophys. Astrophys. Fluid Dyn.* **101** 81

Steenbeck M and Krause F 1969 *Astron. Nachr.* **291** 49

Sur S, Subramanian K and Brandenburg A 2007 *Mon. Not. R. Astron. Soc.* **376** 1238

Sur S, Brandenburg A and Subramanian K 2008 *Mon. Not. R. Astron. Soc.* **385** L15

Tobias S M, Cattaneo F and Brummell N H 2008 *Astrophys. J.* **685** 596

Vishniac E T and Cho J 2001 *Astrophys. J.* **550** 752

Ziegler U and Rüdiger G 2000 *Astron. Astrophys.* **356** 1141